

This discussion paper is/has been under review for the journal Atmospheric Chemistry and Physics (ACP). Please refer to the corresponding final paper in ACP if available.

Technical Note: Spectral representation of spatial correlations in variational assimilation with grid point models and application to the belgian assimilation system for chemical observations (BASCOE)

Q. Errera¹ and R. Ménard²

¹Institut d'Aéronomie Spatiale de Belgique, BIRA-IASB, Belgium

²Environment Canada, Canada

Received: 25 May 2012 – Accepted: 11 June 2012 – Published: 6 July 2012

Correspondence to: Q. Errera (quentin@oma.be)

Published by Copernicus Publications on behalf of the European Geosciences Union.

Spectral representation of background error covariances

Q. Errera and R. Ménard

Title Page

Abstract

Introduction

Conclusions

References

Tables

Figures

⏪

⏩

◀

▶

Back

Close

Full Screen / Esc

Printer-friendly Version

Interactive Discussion

Abstract

The formulation of the background error covariances represented in the spectral space is discussed in the context of univariate assimilation relying on a grid point model, leaving out all the aspects of balances between the different control variables needed in meteorological assimilation. The spectral transform operations are discussed in the case of a spherical harmonics basis and we stress that there is no need for an inverse spectral transform and of a Gaussian grid. The analysis increments are thus produced directly on the model grid. The practice of producing analysis increments on a horizontal Gaussian grid and then interpolating on a equally spaced grid is also shown to produce a degradation of the analysis. The method discussed in this paper allows the implementation of separable and non-separable spatial correlations. The separable formulation has been implemented in the Belgian Assimilation System for Chemical Observations (BASCOE) and its impact on the assimilation of O_3 observed by the Michelson Interferometer for Passive Atmospheric Sounding (MIPAS) is shown. To promote the use of this method by other non-meteorological variational systems and in particular chemistry, the Fortran code developed is made available to the community.

1 Introduction

One of the critical aspects of any assimilation system is the formulation of the background spatial error covariances matrix, denoted the **B** matrix. It needs to be sufficiently compact to be numerically implemented and sufficiently complex to represent correctly the real error covariances of the first guess field. There are several approaches to achieve this goal. For variational systems, which are the systems we will focus on, two approaches have been developed. The first one historically (Parrish and Derber, 1992), which we shall discuss at length in this paper, uses a spectral representation of the correlation matrix. It is based on the fact that a homogeneous and isotropic horizontal correlation matrix can be represented by a diagonal matrix in the spectral

Spectral representation of background error covariances

Q. Errera and R. Ménard

Title Page

Abstract

Introduction

Conclusions

References

Tables

Figures

⏪

⏩

◀

▶

Back

Close

Full Screen / Esc

Printer-friendly Version

Interactive Discussion



space. This property was discovered in the late sixties by Russian scientists working in statistical fluid mechanics and turbulence theory (see the works of Monin and Yaglom, 1971, 1975; Panchev, 1971). These concepts were extended to the sphere and applied successfully to large-scale atmospheric dynamics and analyses by Boer (1983) and Boer and Shepherd (1983) using spherical harmonics as the orthogonal basis. It is only in the late nineties that this formulation became the cornerstone of 3-dimensional variational meteorological assimilation systems (Courtier et al., 1998), and was applied later to chemical data assimilation (Dethof and Hólm, 2004). More recently, efforts have been done to develop spectral representation of inhomogeneous and flow-dependent correlations Fisher (2003).

The second approach for variational systems is based on a diffusion operator which uses the model's diffusion to generate the effect of a Gaussian correlation function. This method was introduced by Derber and Rosati (1989) and further developed by Weaver and Courtier (2001). This method is particularly useful when the domain has complex boundaries (e.g. ocean data assimilation) where it is difficult to define positive definite correlations. This method is also well suited for models that have non uniform grid on a sphere (e.g. icosahedral grids) because it avoids the interpolation of analysis increments onto that grid (Elbern et al., 2010; Schwinger and Elbern, 2010). The diffusion approach primarily gives rise to a Gaussian covariance model but can be generalized to more complex (i.e. inhomogeneous and anisotropic) correlations. However, the diffusion approach is highly demanding in computer resources (both CPU and memory), especially if one needs to simulate non-Gaussian correlations.

This paper discusses the spectral representation of background error correlations onto a spherical harmonic basis. Most of the mathematical background presented in this paper has already been published (see the references cited in Sects. 2–4). However, none of those publications provide a complete picture of the problem. For instance, these publications rarely give an introduction on spectral transformations. As numerical weather prediction (NWP) systems usually rely on spectral models, this aspect is supposed to be known. Moreover, those publications describe the method in

Spectral representation of background error covariances

Q. Errera and R. Ménard

[Title Page](#)[Abstract](#)[Introduction](#)[Conclusions](#)[References](#)[Tables](#)[Figures](#)[Back](#)[Close](#)[Full Screen / Esc](#)[Printer-friendly Version](#)[Interactive Discussion](#)

Spectral representation of background error covariances

Q. Errera and R. Ménard

[Title Page](#)[Abstract](#)[Introduction](#)[Conclusions](#)[References](#)[Tables](#)[Figures](#)[Back](#)[Close](#)[Full Screen / Esc](#)[Printer-friendly Version](#)[Interactive Discussion](#)

the meteorological context, that is the use of balance operators between meteorological variables. This makes the background theory of this method difficult to be acquired for people not involved in meteorology. As a consequence, one of the aims of this paper is to describe the spectral representation of the background error correlations for univariate assimilation with systems relying on a grid point model.

A code for this purpose has been developed and implemented in the Belgian Assimilation System for Chemical Observations (BASCOE). In doing so we have identified a rather important property that seemed to have been overlooked in meteorological data assimilation: in variational assimilation only the adjoint spectral transform is necessary, not the inverse transform. As a result the analysis spectral increments are produced directly on the model grid. In other words, there is no need to extract the increments on the (non-equally spaced) Gaussian grid and then to perform a transformation from that grid to the model grid – a transformation which necessarily degrades the analysis. While this method is limited to homogeneous and isotropic correlations, it has the advantage of being very low demanding in computer resources. Moreover, while not studied in this paper, non-separable three-dimensional error correlations could be implemented easily, meaning that vertical correlations can be different for large and small horizontal spectral features.

This paper is organized as follows. Section 2 and Appendix A introduce representations in spherical harmonics and the spectral representation of homogeneous and isotropic correlations. Section 3 discusses the variational formulation and the control variable change from the model basis to the spherical harmonic basis. The implementation of the spectral transform operators and of the spatial correlations is described in Sect. 4. Section 5 discusses the numerical implementation of the method and illustrates it by the results of an assimilation of a single pseudo-observation. In Sect. 6, the method is applied to real ozone observations using the BASCOE system. The results of this paper are summarized in the conclusions. A Fortran code of this method is provided in the Supplement of this paper. This code is introduced in the Appendix B.

2 Introduction on spectral transform on the sphere

This section provides some useful information about two-dimensional spectral representation on the sphere. For an exhaustive introduction, we refer to the books of Satoh (2004) and Krishnamurti et al. (2006), and the unpublished lectures of P. Swartrauber¹.

In this section, we denote a 2-D field on the sphere by $\Psi(\lambda, \mu)$ where λ is the longitude, $\mu = \sin \phi$ and ϕ is the latitude. Alternatively, the notation Ω will be used in place of (λ, μ) . The field $\Psi(\lambda, \mu)$ can be represented by a series of spherical harmonics where the coefficients are noted Ψ_n^m . The values of n and m are specified below. In this section, the term *grid* will be associated with the *horizontal grid* and not the usual three dimensional grid of the model.

2.1 Spherical harmonics

Spherical harmonics, denoted by Y_n^m , are defined as solutions of the Laplace equation. They take the following form:

$$Y_n^m(\lambda, \mu) = N_n^m P_n^m(\mu) e^{im\lambda} \quad (1)$$

where N_n^m are the normalization constants, $P_n^m(\mu)$ are the *associated Legendre functions* and $e^{im\lambda}$ are the Fourier exponentials where $i^2 = -1$. Spherical harmonics form an orthogonal basis and their normalization is defined by the normalization constants. This is discussed in detail in Appendix A1. Here the geodesy 2π normalization is adopted (while Courtier et al., 1998, uses the geodesy 4π) such that:

$$\int_{-\pi-1}^{\pi+1} \int Y_n^m(\lambda, \mu) (Y_{n'}^{m'}(\lambda, \mu))^* \mathbf{d}\mu \mathbf{d}\lambda = 2\pi \delta_n^{n'} \delta_m^{m'} \quad (2)$$

¹Available at: www.cisl.ucar.edu/css/staff/pauls/tutorials/index.html

Spectral representation of background error covariances

Q. Errera and R. Ménéard

Title Page

Abstract

Introduction

Conclusions

References

Tables

Figures

⏪

⏩

◀

▶

Back

Close

Full Screen / Esc

Printer-friendly Version

Interactive Discussion



where $(.)^*$ denotes the complex conjugate and $\delta_k^{k'}$ is the Kronecker symbol ($\delta_k^{k'} = 1$ if $k = k'$ and 0 otherwise). When $m = 0$, P_n^0 are called the *Legendre polynomials*. In such a case the value of m is omitted in the notation ($P_n^0 \equiv P_n$). When spherical harmonics are used in the context of spectral transforms, as in this study, it is appropriate to include the normalization constant in the associated Legendre functions. In this case, we define the *normalized associated Legendre functions* as $\bar{P}_n^m(\mu) \equiv N_n^m P_n^m(\mu)$.

2.2 Direct spectral transform

In general, a smooth function on a sphere $\Psi(\lambda, \mu)$ can be represented by a series of spherical harmonics with coefficients Ψ_n^m :

$$\Psi(\lambda, \mu) = \sum_{n=0}^{\infty} \sum_{m=-n}^n \Psi_n^m Y_n^m(\lambda, \mu). \quad (3)$$

In this transformation, and recalling the definition of the spherical harmonics (Eq. 1), the dependence along the longitude is taken by the Fourier exponentials. For this reason, m is called the *zonal wavenumber*. In addition, n is called the *total wavenumber*.

Ψ_n^m are complex coefficients. If $\Psi(\lambda, \mu)$ is real, which is the case in atmospheric sciences, then the following property holds:

$$\Psi_n^m = (-1)^m (\Psi_n^{-m})^*. \quad (4)$$

This suggests that it might be possible to define real coefficients using Fourier sine and cosine instead of the complex coefficients using Fourier exponentials. In this study, the complex representation is kept.

The transform Eq. (3) cannot be evaluated exactly and requires to be truncated at some reasonable number of terms. Several truncation methods exist and here the triangular truncation is adopted. In this case, the relationship between the spectral

Spectral representation of background error covariances

Q. Errera and R. Ménéard

Title Page

Abstract

Introduction

Conclusions

References

Tables

Figures

⏪

⏩

◀

▶

Back

Close

Full Screen / Esc

Printer-friendly Version

Interactive Discussion



coefficients and the physical field is given by

$$\Psi(\lambda_j, \mu_k) = \sum_{n=0}^N \sum_{m=-n}^n \Psi_n^m \bar{P}_n^m(\mu_k) e^{im\lambda_j} \quad (5)$$

$$= \sum_{m=-N}^N \sum_{n=|m|}^N \Psi_n^m \bar{P}_n^m(\mu_k) e^{im\lambda_j} \quad (6)$$

5 where N is the degree of truncation (and should not be confused with the normalization factor N_n^m) and where j and k are, respectively the longitude and latitude indices of the spectral grid. For practical purposes, Eq. (6) is split in a Fourier transform followed by a Legendre transform:

$$\Psi^m(\mu_k) = \sum_{n=|m|}^N \Psi_n^m \bar{P}_n^m(\mu_k) \quad (7)$$

$$10 \Psi(\lambda_j, \mu_k) = \sum_{m=-N}^N \Psi^m(\mu_k) e^{im\lambda_j} . \quad (8)$$

2.3 Inverse spectral transform

Given a 2-D field $\Psi(\lambda, \mu)$ on the sphere, the question is now how we can calculate its spectral coefficients Ψ_n^m . Using the orthogonality of the spherical harmonics, the
 15 inverse of Eq. (3) is given by

$$\Psi_n^m = \frac{1}{2\pi} \int_0^{2\pi} \int_{-1}^1 \Psi(\lambda, \mu) (Y_n^m(\lambda, \mu))^* \mathbf{d}\mu \mathbf{d}\lambda . \quad (9)$$

In order to solve this equation, one usually starts with a discrete 2-D field given on a grid $\Psi(\lambda_j, \mu_k)$ and looks to invert the sequence (Eqs. 7, 8). The inverse of the Fourier

Spectral representation of background error covariances

Q. Errera and R. Ménard

Title Page

Abstract

Introduction

Conclusions

References

Tables

Figures

◀

▶

◀

▶

Back

Close

Full Screen / Esc

Printer-friendly Version

Interactive Discussion



transform (Eq. 8) is given by:

$$\Psi^m(\mu_k) = \frac{1}{M} \sum_{j=0}^{M-1} \Psi(\lambda_j, \mu_k) e^{-im\lambda_j} \quad (10)$$

where M is the number of longitudes.

The inverse of the Legendre transform (Eq. 7) is much more difficult to implement.

5 One aspect that has not been addressed yet is the specification of the *spectral grid*, i.e. what we define as the target grid of the spectral transform. The direct transform (Eqs. 7, 8) and the inverse of the Fourier transform (Eq. 10) are applicable to any type of spectral grid, in particular the equally spaced (in degree) model grid. However, this is not true for the inverse of the Legendre transform. If one needs to calculate
 10 the exact inverse of Eq. (7) without loss of information, the choice of spectral grid is limited to the *Gaussian grid*. On this grid, the latitudes correspond to the roots of the Legendre polynomials $P_N(\mu_k) = 0$, which are not equally spaced. The longitudes, on the other hand, are equally spaced. On the Gaussian grid, the inverse spectral transform is defined by the following *Gaussian quadrature* (see the proof in Krishnamurti et al.,
 15 2006, Sect. 6.6; or Satoh, 2004, Sect. 21.3):

$$\Psi_n^m = \sum_{k=1}^K w(\mu_k) \Psi^m(\mu_k) \bar{P}_n^m(\mu_k) \quad (11)$$

where K is the number of latitudes and $w(\mu_k)$ are the Gaussian weights which can be calculated analytically.

20 While the Gaussian grid allows to define an exact inverse transform, an accurate (but not exact) inverse transform can also be defined from the equally spaced grid. This is reported in the Appendix A2.

Spectral representation of background error covariances

Q. Errera and R. Ménard

Title Page	
Abstract	Introduction
Conclusions	References
Tables	Figures
⏪	⏩
◀	▶
Back	Close
Full Screen / Esc	
Printer-friendly Version	
Interactive Discussion	



2.4 Adjoint spectral transform

In variational assimilation where the \mathbf{B} matrix is defined in the spectral space, the adjoint of the spectral transform (Eqs. 7, 8) is needed. Let us denote the spectral transform operator by \mathbf{S} . To obtain the gradient of the cost function (see Sect. 3), one needs to define the adjoint of \mathbf{S} , denoted by \mathbf{S}^* (that must not be confused with the conjugate operator $(\cdot)^*$). Since $\Psi(\lambda, \mu)$ is real, we have $\mathbf{S}^* = \mathbf{S}^T$. One way to implement the adjoint is to (re)define the spectral transform as unitary operations such that $\mathbf{S}^{-1} = \mathbf{S}^T$. This is possible by re-writing the direct spectral transform (Eqs. 7, 8) as

$$\Psi^m(\mu_k) = \sqrt{\frac{1}{M}} \sum_{n=|m|}^N \Psi_n^m \bar{P}_n^m(\mu_k) \quad (12)$$

$$\Psi(\lambda_j, \mu_k) = \sum_{m=-N}^N \sqrt{w(\mu_k)} \Psi^m(\mu_k) e^{im\lambda_j}, \quad (13)$$

and the inverse spectral transform (Eqs. 10, 11) as

$$\Psi^m(\mu_k) = \sqrt{\frac{1}{M}} \sum_{j=0}^{M-1} \Psi(\lambda_j, \mu_k) e^{-im\lambda_j} \quad (14)$$

$$\Psi_n^m = \sum_{k=1}^K \sqrt{w(\mu_k)} \Psi^m(\mu_k) \bar{P}_n^m(\mu_k). \quad (15)$$

However, this formulation requires the use of the Gaussian grid as the spectral grid. If one uses a model defined on an equally spaced grid, as usually done in atmospheric modeling, a mapping operation will be necessary to map the analysis increments from the spectral grid to the model grid. As mapping operations introduce a degradation of the increments, it is better to find an alternative to the unitary definition of the spectral transforms. For this reason, the adjoint of the code of the direct spectral transform

Spectral representation of background error covariances

Q. Errera and R. Ménéard

Title Page

Abstract

Introduction

Conclusions

References

Tables

Figures

◀

▶

◀

▶

Back

Close

Full Screen / Esc

Printer-friendly Version

Interactive Discussion



sequence (Eqs. 7, 8) has been written by hand in BASCOE. In terms of equation, the operator \mathbf{S}^* takes the form:

$$\Psi^m(\mu_k) = \sum_{j=0}^{M-1} \Psi(\lambda_j, \mu_k) e^{-im\lambda_j} \quad (16)$$

$$\Psi_n^m = \sum_{k=1}^K \Psi^m(\mu_k) \bar{P}_n^m(\mu_k). \quad (17)$$

2.5 Degree of truncation, spectral grid and aliasing

To complete the definition of the spectral operators, we have to define a degree of truncation N and the corresponding dimensions of the horizontal spectral grid M and K . First, let us consider the unitary definition of the spectral transforms. In order to keep the information content equal in a sequence of direct and inverse Fourier transforms, one needs to impose that $M = 2(N + 1)$ (Krishnamurti et al., 2006, Chap. 7; Swarztrauber, Lecture 1). If one tries $M > 2(N + 1)$, a false representation, or *aliasing* is introduced. On the other hand, if $M < 2(N + 1)$, there is a loss of information during the spectral transform (i.e. the spectral representation has a higher resolution than the spectral grid). Aliasing in the associated Legendre functions also exists but is much more difficult to derive. Associated Legendre functions can be obtained by a sum of Fourier coefficients in the latitude direction (Swarztrauber, Lecture 2). In this case, the aliasing is prevented if $K \leq N + 1$ and the equality is required for no loss of information in a sequence of direct and inverse Legendre transform.

If one bases their code on the non-unitary spectral transforms, the condition is less strict. It can be verified with the code provided in the Supplement of this paper that the following conditions must hold: $N \geq \max(K, M/2) - 1$. This allows to implement longitudes and latitudes that have not necessarily the same resolution, which is usually the case in atmospheric modelling.

Spectral representation of background error covariances

Q. Errera and R. Ménard

Title Page

Abstract

Introduction

Conclusions

References

Tables

Figures

⏪

⏩

◀

▶

Back

Close

Full Screen / Esc

Printer-friendly Version

Interactive Discussion



In the case of the BASCOE horizontal grid of $2^\circ \times 2^\circ$ that includes the poles (as done in Sect. 6), the model resolution is 91 latitudes and 180 longitudes. If the spectral grid is the BASCOE model grid, $K = 91$, $M = 180$ and the degree of truncation is fixed to $N = 90$. If the spectral grid is the Gaussian grid, a mapping operator \mathbf{G} must be introduced to account for the transformation from the Gaussian grid to the BASCOE grid. In this case, the size of the Gaussian grid is $K = 90$ and $M = 180$, the degree of truncation is $N = 89$ and the dimensions of \mathbf{G} are 90×89 .

2.6 Spectral representation of spatial correlations

Let $\epsilon(\Omega)$ be an error field on the surface sphere where $\Omega = (\lambda, \mu)$. Let us assume that the error field is unbiased and normalized, i.e. $\langle \epsilon(\Omega)^2 \rangle = 1$ where $\langle \rangle$ denotes the mathematical expectation. Let us assume that the correlations are homogeneous and isotropic. This means that the correlations between the points Ω and Ω' depends only on the distance \mathbf{d} between the two points. Gaspari and Cohn (1999) have shown that, on a sphere of radius A , \mathbf{d} corresponds to the *chordal* or *geodetic* distance between the two points

$$d \equiv d(\theta) = A\sqrt{2(1 - \cos \theta)}.^2 \quad (18)$$

where θ is their angular separation as defined in Eq. (A14). It follows that the correlations between the two points might be expressed as a function of θ :

$$\langle \epsilon(\Omega)\epsilon(\Omega') \rangle = f(\theta). \quad (19)$$

The concept of homogeneous and isotropic correlations on the surface of a sphere is however not independent as noted by Gaspari and Cohn (1999), and needs to be somewhat revised. Isotropy can be obtained by translation invariance back to the same point along great circle with translations in any directions – so basically the correlation

²And not $2\sqrt{(1 - \cos \theta)}$ as reported in Gaspari and Cohn (1999, Eq. 2.33).

Spectral representation of background error covariances

Q. Errera and R. Ménard

Title Page

Abstract

Introduction

Conclusions

References

Tables

Figures

⏪

⏩

◀

▶

Back

Close

Full Screen / Esc

Printer-friendly Version

Interactive Discussion



function only need to be homogeneous. Also as discussed in the same paper, any homogeneous correlation function defined in \mathbb{R}^3 is also homogeneous on any continuous manifold imbedded in \mathbb{R}^3 , such as the surface of a sphere. Thus an homogeneous (translation invariant) correlation function on the surface of a sphere can be defined from a correlation using as a distance, the distance \mathbf{d} defined in \mathbb{R}^3 that is the chordal distance (and not the great circle distance), and which has the consequence to be implicitly periodic from all directions.

Coming back to Eq. (19) and supposing that one of the two points is at the north pole, then θ is the co-latitude angle, i.e. $\theta \equiv \frac{\pi}{2} - \phi$. Consequently, we have $\cos \theta = \mu$. Placing one of the two points at the north pole makes the correlations between the two points independent of the longitude. If f_n^m represents the spectral coefficients of $f(\theta)$, we have $f_n^m = 0$ for $m \neq 0$. It follows that

$$f(\theta) = \sum_{n=0}^N \sum_{m=-n}^n f_n^m Y_n^m(\lambda, \cos \theta) \quad (20)$$

$$= \sum_{n=0}^N f_n \bar{P}_n^m(\cos \theta) \quad (21)$$

where $f_n \equiv f_n^0$. Boer (1983); Gauthier et al. (1993) have shown that the correlations are represented by a diagonal matrix on a spherical harmonics basis, i.e.

$$\langle \epsilon_n^m \epsilon_{n'}^{m'} \rangle = b_n \delta_n^{n'} \delta_m^{m'} \quad (22)$$

where $b_n \equiv f_n / N_n^0$ (see also the proof in Appendix A4).

3 Variational assimilation and control variable transform

Variational methods (three-dimensional – 3D-Var – and four-dimensional – 4D-Var) aim at calculating the model state that minimizes the objective function $J(\mathbf{x})$ (Talagrand,

Spectral representation of background error covariances

Q. Errera and R. Ménard

Title Page

Abstract

Introduction

Conclusions

References

Tables

Figures

⏪

⏩

◀

▶

Back

Close

Full Screen / Esc

Printer-friendly Version

Interactive Discussion



1997):

$$J(\mathbf{x}) = J^b(\mathbf{x}) + J^o(\mathbf{x}) \quad (23)$$

where

$$J^b(\mathbf{x}) = \frac{1}{2}[\mathbf{x} - \mathbf{x}^b]^T \mathbf{B}^{-1}[\mathbf{x} - \mathbf{x}^b] \quad (24)$$

$$J^o(\mathbf{x}) = \frac{1}{2}[\mathbf{y} - H(\mathbf{x})]^T \mathbf{R}^{-1}[\mathbf{y} - H(\mathbf{x})], \quad (25)$$

where \mathbf{x}^b and \mathbf{B} are, respectively the background model state (i.e. the initial guess) and its associated error covariance matrix; \mathbf{y} and \mathbf{R} are, respectively the observational vector and its associated error covariance matrix; \mathbf{x} is the model state vector and H is the non-linear observation operator that projects the model state in the observation space. In the 3D-Var case the observations and the model state correspond to the same time. In the 4D-Var case, observations span over an assimilation time window, the model state \mathbf{x} is defined at the beginning of that window (or initial time) and the observation operator H includes an evolution model operator that projects the model initial state \mathbf{x} at the observation time.

The minimization of Eq. (23) is usually done with a quasi-Newton minimizer that requires the knowledge of the gradient of the objective function:

$$\nabla_{\mathbf{x}} J = \frac{\partial J}{\partial \mathbf{x}} = \nabla_{\mathbf{x}} J^b + \nabla_{\mathbf{x}} J^o \quad (26)$$

$$\nabla_{\mathbf{x}} J^b = \mathbf{B}^{-1}[\mathbf{x} - \mathbf{x}^b] \quad (27)$$

$$\nabla_{\mathbf{x}} J^o = \left(\frac{\partial H(\mathbf{x})}{\partial \mathbf{x}} \right)^T \mathbf{R}^{-1}[\mathbf{y} - H(\mathbf{x})]. \quad (28)$$

As the typical dimension of \mathbf{x} is around 10^6 , the matrix \mathbf{B} is of size 10^{12} . This is far too large to be stored and inverted by modern computers. Moreover, the specification

16775

Spectral representation of background error covariances

Q. Errera and R. Ménard

Title Page

Abstract

Introduction

Conclusions

References

Tables

Figures

⏪

⏩

◀

▶

Back

Close

Full Screen / Esc

Printer-friendly Version

Interactive Discussion



of the elements of such a matrix requires a huge amount of a priori information, more than available (Dee, 1995). For those reasons, it is necessary to reduce the problem. Here, we follow the same strategy as developed at ECMWF in late nineties (Courtier et al., 1998). A review on the formulation of background error covariance matrix in meteorology might be found in Bannister (2008a,b).

In order to avoid the problem of inverting \mathbf{B} , a control variable transform is introduced:

$$\mathbf{L}\chi = \underbrace{\mathbf{x} - \mathbf{x}^b}_{\delta\mathbf{x}} \quad (29)$$

where χ is a new control variable, $\delta\mathbf{x}$ is the analysis increment and \mathbf{L} is the square root of \mathbf{B} :

$$\mathbf{B} = \mathbf{L}^T \mathbf{L} . \quad (30)$$

The objective function thus becomes:

$$J^b(\chi) = \frac{1}{2} \chi^T \chi \quad (31)$$

$$J^o(\chi) = \frac{1}{2} [\mathbf{d} - H(\mathbf{L}\chi)]^T \mathbf{R}^{-1} [\mathbf{d} - H(\mathbf{L}\chi)] \quad (32)$$

where

$$\mathbf{d} = \mathbf{y} - H(\mathbf{x}^b) \quad (33)$$

is the innovation vector. The background term (Eq. 31) can be easily calculated. If the observation operator H is linear, the term $\mathbf{d} - H(\mathbf{L}\chi)$ in Eq. (32) is equal to the term $\mathbf{y} - H(\mathbf{x})$ in Eq. (25). As a result, $J^o(\mathbf{x}) = J^o(\chi)$. If H is non-linear but the difference $\mathbf{x} - \mathbf{x}^b$ is small, then H can be linearized. It follows that the calculation of J^o is practically obtained by the resolution of Eq. (25), which is much easier to implement numerically than Eq. (32).

Spectral representation of background error covariances

Q. Errera and R. Ménard

Title Page

Abstract

Introduction

Conclusions

References

Tables

Figures

⏪

⏩

◀

▶

Back

Close

Full Screen / Esc

Printer-friendly Version

Interactive Discussion



The gradient of the objective function is now given by:

$$\nabla_{\chi} J^b = \chi \quad (34)$$

$$\nabla_{\chi} J^o = \mathbf{L}^* \left(\frac{\partial H(\chi)}{\partial \chi} \right)^T \mathbf{R}^{-1} [\mathbf{d} - H(\mathbf{L}\chi)] \quad (35)$$

5 where \mathbf{L}^* is the adjoint of the operator \mathbf{L} . Again, the calculation of the background term (Eq. 34) of the gradient is no longer an issue and it can be verified that the gradient of the observation term (Eq. 35) corresponds to the operator \mathbf{L}^* applied to the results of Eq. (28), i.e. $\nabla_{\chi} J^o = \mathbf{L}^* \nabla_{\mathbf{x}} J^o$. With χ as the control variable, the iterative sequence of operations necessary to minimize J is:

- 10 1. Initialization: read \mathbf{x}^b and \mathbf{y} , set $\chi = 0$
2. Calculate J^b by Eq. (31)
3. Get $\mathbf{x} = \mathbf{L}\chi + \mathbf{x}^b$ and calculate J^o by Eq. (25)
4. Get $J = J^b + J^o$
5. Calculate $\nabla_{\chi} J^b$ by Eq. (34)
- 15 6. Calculate $\nabla_{\mathbf{x}} J^o$ by Eq. (28)
7. Get $\nabla_{\chi} J = \nabla J^b + \mathbf{L}^* \nabla_{\mathbf{x}} J^o$
8. Provide χ , J and $\nabla_{\chi} J$ to the minimizer and update χ
9. If convergence, get $\mathbf{x} = \mathbf{L}\chi + \mathbf{x}^b$ and start a forecast until the next analysis time. Otherwise, go to step 3.

Spectral representation of background error covariances

Q. Errera and R. Ménard

Title Page

Abstract

Introduction

Conclusions

References

Tables

Figures

⏪

⏩

◀

▶

Back

Close

Full Screen / Esc

Printer-friendly Version

Interactive Discussion



4 Formulation of \mathbf{L} and its adjoint \mathbf{L}^*

By definition, the background error covariance matrix \mathbf{B} is the product of a standard deviation error matrix $\mathbf{\Sigma}$ (diagonal) and a correlation matrix \mathbf{C} (non diagonal):

$$\mathbf{B} = \mathbf{\Sigma}\mathbf{C}\mathbf{\Sigma} \quad (36)$$

5 or

$$\mathbf{L} = \mathbf{\Sigma}\mathbf{C}^{1/2} . \quad (37)$$

In this study, we will only deal with univariate correlations such that no species-species correlations are considered in BASCOE. As the matrix $\mathbf{C}^{1/2}$ is huge, it is necessary to make assumptions and/or transformations to allow its implementation in a variational system (see Sect. 1). In the NWP community, it was suggested to build the correlation matrix in the spectral space (see e.g. Courtier et al., 1998). As mentioned in Sect. 2.6, assuming homogeneous and isotropic horizontal correlations at the surface of a sphere allows to get a diagonal correlation matrix in the spectral space. This means that considering a 3-D model on the sphere, the spatial correlations are then represented by a block diagonal matrix. Let $\mathbf{\Lambda}^{1/2}$ denote the spectral representation of $\mathbf{C}^{1/2}$ and \mathbf{S} the spectral transform operator. Hence, the transformation $\mathbf{C}^{1/2}$ can be rewritten as $\mathbf{S}\mathbf{\Lambda}^{1/2}$, so that \mathbf{L} becomes:

$$\mathbf{L} = \mathbf{\Sigma}\mathbf{G}\mathbf{S}\mathbf{\Lambda}^{1/2} . \quad (38)$$

The operator \mathbf{G} has been introduced in Eq. (38) to account for the transformation from the spectral grid to the model grid. In the case where the analysis increments are calculated on the Gaussian grid, the transformation \mathbf{G} is represented by a weighting average over the latitudes. In the case where the spectral grid is the model grid, no transformation is implemented (\mathbf{G} is the identity matrix).

Spectral representation of background error covariances

Q. Errera and R. Ménéard

Title Page

Abstract

Introduction

Conclusions

References

Tables

Figures

⏪

⏩

◀

▶

Back

Close

Full Screen / Esc

Printer-friendly Version

Interactive Discussion



The adjoint operator \mathbf{L}^* is given by

$$\mathbf{L}^* = \mathbf{\Lambda}^{1/2} \mathbf{S}^* \mathbf{G}^* \mathbf{\Sigma} . \quad (39)$$

Recall that $\mathbf{\Lambda}$ is a symmetric block diagonal matrix and that $\mathbf{\Sigma}$ is a diagonal matrix, so the transpose sign $(.)^T$ has been omitted for these matrices in the equations.

The block diagonal elements of $\mathbf{\Lambda}$ have the dimensions $L \times L$ where L is the number of vertical levels of our model. Each element of a block $\mathbf{\Lambda}_n^m$ takes the form

$$\Lambda_n^m(p, p') = \sqrt{b_n(p)b_n(p')} C_n^v(p, p') \quad (40)$$

where the coefficients b_n are those of Eq. (22) (Berre, 2000, see also the Appendix A4). This is the non-separable formulation of the spatial correlations. By this formulation of $\mathbf{\Lambda}$, the horizontal correlation coefficients b_n are dependent on the altitude. Moreover, the matrices \mathbf{C}_n^v allow to take into account different vertical correlations for different wavenumbers. In other words, features with large horizontal scale could have different vertical correlations than features of small horizontal scale (Fisher, 2003). This specification is necessary in meteorology in order to get correct correlations between the mass and wind fields (Phillips, 1986; Bartello and Mitchell, 1992) while this non-separability has never been studied in chemistry data assimilation yet. Note that the vertical correlation matrices \mathbf{C}_n^v are defined independently of the zonal wavenumber m , as found for the horizontal correlation coefficients b_n . This formulation of the background matrix is then very low demanding in computer resources.

Although this non-separability formulation could be implemented in the present formulation of the correlation matrix $\mathbf{\Lambda}$ in BASCOE, this has not been done in this study. Here, we have assumed that horizontal and vertical correlations are separable, i.e.

$$\mathbf{\Lambda}_n^m = b_n \mathbf{C}_n^v \quad (41)$$

where the horizontal correlation coefficients are taken independent on the altitude and where the vertical correlation matrix are independent on the wavenumber n .

Spectral representation of background error covariances

Q. Errera and R. Ménard

Title Page

Abstract

Introduction

Conclusions

References

Tables

Figures

⏪

⏩

◀

▶

Back

Close

Full Screen / Esc

Printer-friendly Version

Interactive Discussion



Spectral representation of background error covariances

Q. Errera and R. Ménéard

Title Page

Abstract

Introduction

Conclusions

References

Tables

Figures

◀

▶

◀

▶

Back

Close

Full Screen / Esc

Printer-friendly Version

Interactive Discussion

Usually, the b_n coefficients and the vertical correlations matrices \mathbf{C}_n^v are estimated or *calibrated* in order to match the statistical a priori errors of an assimilation system. This can be done using methods that allow to derive an ensemble of error fields from which these statistics are calculated. We will not describe all these calibration methods and will refer to Bannister (2008a, Sect. 5) for a complete review. In the current study, the correlation matrix of BASCOE has not been calibrated. Instead, a priori correlation functions have been used to build it. In the code provided in the Supplement, two functions have been coded for the horizontal correlations: a Gaussian function

$$f(\theta) = \exp\left(-\frac{1 - \cos\theta}{L^2}\right) \quad (42)$$

and a second-order autoregressive (SOAR) function

$$f(\theta) = \left(1 + \frac{2\sqrt{1 - \cos\theta}}{L}\right) \exp\left(-\frac{2\sqrt{1 - \cos\theta}}{L}\right) \quad (43)$$

where $L = L_h/A_0$, A_0 is the Earth's radius and L_h is a horizontal correlation length scale.

For the vertical correlations, again, two functions are coded: a *hat* function

$$C^v(p_i, p_j) = \begin{cases} 1 & \text{for } i = j \\ 1/2 & \text{for } |i - j| = 1 \\ 0 & \text{for } |i - j| > 1 \end{cases} \quad (44)$$

and a Gaussian function

$$C^v(p_i, p_j) = \exp\left(-\frac{1}{2} \left(\frac{|p_i - p_j|}{L_v}\right)^2\right). \quad (45)$$

For the Gaussian case, the distance between two levels $|p_i - p_j|$ can either be measured in level indices or in kilometers. Moreover, a correlation length scale L_v must be provided in the same units as p .

Finally, the square root of \mathbf{C}^V , which is necessary to build $\mathbf{\Lambda}^{1/2}$ (see Eqs. 38 and 39), is obtained by a singular value decomposition (SVD).

5 Assimilation of a single pseudo-observation

The operators described in Sect. 4 have been implemented in Fortran and tested. This code is provided in a Supplement to this paper. It includes the code for the different operators that define \mathbf{L} and \mathbf{L}^* , as well as two tests. All this material is introduced in Appendix B.

This section presents the results of an assimilation of a single pseudo-observation using the 3D-Var method. The goal is to evaluate the implementation of the \mathbf{B} matrix by an assimilation for which the result is theoretically known. Here, we choose to assimilate a pseudo-observation with a value of 1.2 and located at a model grid point. The background field \mathbf{x}^b has a constant value of 1. Both the observation and the background field have an error standard deviation of 0.1. The optimization is done by the quasi-Newton algorithm M1QN3 (Gilbert and Lemarechal, 1989). This test has been performed using two spectral grids: an equally spaced grid (denoted the lat/lon) and a Gaussian grid. Several model resolutions, and locations of the observation and (horizontal and vertical) correlation functions have been considered in these tests. Here are shown only the results obtained with a particular but representative configuration of the experiment. This configuration considers a Gaussian correlation function with correlation length scales L_h of 600 km horizontally and L_v of 3 model levels vertically. The resolution of the model is 120 longitudes by 60 latitudes by 31 levels and the degree of truncation is 59. The observation is placed at the grid point indice (60,30,16) in (lon,lat,lev), i.e. close to the Equator and at the middle level. In such a configuration, the theoretical analysis at the observation location is 1.1. From that point, the analysis should decrease according to a Gaussian bell curve with a standard deviation that corresponds to the correlation length scales, i.e. 600 km horizontally and 3 levels vertically.

Spectral representation of background error covariances

Q. Errera and R. Ménard

Title Page

Abstract

Introduction

Conclusions

References

Tables

Figures

⏪

⏩

◀

▶

Back

Close

Full Screen / Esc

Printer-friendly Version

Interactive Discussion



In the following part of this section, the analyses obtained using the Gaussian and the lat/lon grid will be denoted GG and LL, respectively.

Figure 1 displays the results of this test using the two available spectral grids. It shows three cross-sections of the analyses – along the latitude, the longitude and the vertical directions, all of them crossing the observed location. Both analyses present a maximum at the observed locations. As the distance to the observation location increases, the analyses decrease with a Gaussian shape. The GG analysis has a value at the observation point which is significantly different than the expected value of 1.1. On the other hand, the LL analysis is (visually) closer to this expected value. (Note that the theoretical cross-sections are not shown as the LL analyses overlapped them almost entirely.)

Table 1 reports several scores obtained by the two analyses and compares them to the expected theoretical values. For each (computed or theoretical) analysis, the table provides the value of the objective function J , the analysis value at the observation point $H(\mathbf{x})$ and the correlation length scales estimated by a fit of the cross-section lines in Fig. 1 by a Gaussian function. The table also provides the value of the root mean square (RMS) of the differences between the analyzed and the theoretical cross-section. Compared with the GG analysis, the values of J , $H(\mathbf{x})$ and RMS from the LL analysis are closer to the expected value. The correlation length scales obtained by both analyses are close to each other. We have also noted that the “fitted” correlation length scales are slightly different to the expected values, around 575 km instead of 600 horizontally and 2.88 levels instead of 3 vertically. The reason for these deviations is not known. This issue has not been investigated as we found satisfactory the results of the single assimilation experiments as well as the results of real data assimilation (see Sect. 6).

Another way of comparing both analyses is to look at the power spectrum of their increments, which are displayed at the model level of the observation location (Fig. 2a). Recall that the analysis increments are the difference between the analysis and the background field and measure the impact of the observations on the analyses. We

Spectral representation of background error covariances

Q. Errera and R. M enard

Title Page

Abstract

Introduction

Conclusions

References

Tables

Figures

⏪

⏩

◀

▶

Back

Close

Full Screen / Esc

Printer-friendly Version

Interactive Discussion



see that the information provided by the increments differs according to the wavenumber. This is even clearer when the horizontal correlation length scale decreases up to 300 km, i.e. a value closer to the resolution of the grid in the region of the observation (Fig. 2b). At low frequencies (high horizontal scales), the GG analysis provides more information but decreases more rapidly than the LL analysis, this later providing more information at high frequencies (i.e. small horizontal scales). This points out the degradation of the resolution in the analyses due to the transformation **G** from the Gaussian grid to the model grid used in the GG run.

6 Assimilation of real data

In this section, the results of two chemical data assimilation experiments are presented. The first one includes correlations in the **B** matrix while the second one considers a diagonal **B**. The experiments have been performed by means of the 4D-Var Belgian Assimilation System for Chemical Observations (BASCOE, Errera et al., 2008). In its usual configuration, this system considers 57 stratospheric species advected by the Flux-Form Semi-Lagrangian scheme (Lin and Rood, 1996), 200 chemical reactions and a parameterization of the physico-chemical processes due to the so-called Polar Stratospheric Clouds (PSCs). However, in this study, only the advection of ozone is considered (i.e. the chemical and PSC schemes have been turned off) in order to reduce the CPU time. By doing this, it is assumed that ozone behaves like an inert tracer. This is a fair assumption by choosing an assimilation window of one day and by excluding observations above 1 hPa where the ozone time scale is shorter than the assimilation window.

The horizontal resolution is set to $2^\circ \times 2^\circ$ lat/lon grid. This is higher than past experiments based on $3.75^\circ \times 5^\circ$ lat/lon (Geer et al., 2006; Errera et al., 2008; Viscardy et al., 2010) or $2.5^\circ \times 3.75^\circ$ lat/lon grid (Lahoz et al., 2011, and the BASCOE Near Real Time service – <http://macc.aeronomie.be>). The vertical grid is represented by the BASCOE usual 37 vertical levels from the surface to 0.1 hPa, these levels being a subset of the

Spectral representation of background error covariances

Q. Errera and R. Ménard

Title Page

Abstract

Introduction

Conclusions

References

Tables

Figures

⏪

⏩

◀

▶

Back

Close

Full Screen / Esc

Printer-friendly Version

Interactive Discussion



Spectral representation of background error covariances

Q. Errera and R. M enard

Title Page

Abstract

Introduction

Conclusions

References

Tables

Figures

⏪

⏩

◀

▶

Back

Close

Full Screen / Esc

Printer-friendly Version

Interactive Discussion



ECMWF levels. In these experiments, the dynamics is provided by the European Centre for Medium-Range Weather Forecasts (ECMWF) ERA-Interim analyses (Dee et al., 2011). The assimilated ozone data are taken by the Michelson Interferometer for Passive Atmospheric Sounding (MIPAS) ESA off-line level 2 profiles between August and

5 October 2003, as in BASCOE past experiments discussed by Geer et al. (2006) and Errera et al. (2008). MIPAS is a limb fourier transform spectrometer onboard the Envisat platform operating between 2002 and 2012. Measuring in the infrared, limb scans are inverted to provide profiles of numerous trace gases, including ozone (Fischer et al., 2008).

10 Both experiments described in this paper consider 30 % standard deviation in the background fields. The experiment in which spatial correlations are introduced – denoted CORREL – considers a Gaussian correlation function in the horizontal and vertical directions with a correlation length scale $L_h = 600$ km and $L_v = 1$ level, respectively. The experiment using a diagonal \mathbf{B} is denoted DIAG.

15 Figure 3 shows the Observations-minus-Forecast (OmF) statistics for both runs and for the period of the 2003 Antarctic ozone hole (September–October 2003) and for five latitude bands as explained in Errera et al. (2008, Sect. 3.4). Generally, the biases of the OmF obtained by the CORREL run are lower than those obtained by the DIAG run. This is significant in the upper troposphere/lower stratosphere (UTLS) region, between

20 70 and 300 hPa, particularly so in the southern polar region. Regarding the standard deviations, the statistics of both runs are very similar except at the South Pole.

To understand the origin of the differences between both runs, their analysis increments on September 15 at ~ 44 hPa (i.e. at model level 21) are shown in Fig. 4. In the DIAG increments, the track of the satellite is clearly visible and the increments are confined around the observation locations. On the other hand, the CORREL increments are spread over a much larger area, especially in southern high latitudes, thanks to the non-diagonal nature of \mathbf{B} . As shown by the OmF statistics, this improves the assimilation.

25

Spectral representation of background error covariances

Q. Errera and R. Ménard

Title Page

Abstract

Introduction

Conclusions

References

Tables

Figures

⏪

⏩

◀

▶

Back

Close

Full Screen / Esc

Printer-friendly Version

Interactive Discussion



To assess the improvements at the southern high latitudes brought by the non-diagonal \mathbf{B} , both experiments have been compared with ozonesonde observations at three NDACC (Network for the Detection of Atmospheric Composition Change) stations in Antarctica (Amundsen-Scott, Mac Murdo and Neumayer). Figure 5 presents the time series of the ozone partial column between 10 and 100 hPa during the formation of the ozone hole in the 2003 Antarctic winter, along with the corresponding partial column from the analyses. As expected, the CORREL runs agree much better with the observations than the DIAG run. As a result, CORREL exhibits a deeper ozone hole than DIAG which is in better agreement with observations provided by the Total Ozone Mapping Spectrometer (TOMS) (Fig. 6).

The comparison of both runs against ozone sondes in the UTLS has not revealed any “winner” or “looser” (not shown). The possible reasons are that (1) MIPAS observations are of lower quality in the UTLS. Around 100 hPa, it has been found that MIPAS O_3 values are 5 % to 25 % larger compared to the majority of the other datasets (Cortesi et al., 2007). Thus, it would be difficult to find an independent O_3 dataset allowing to assess the improvements brought by the non-diagonal \mathbf{B} . Moreover, (2) the parameters of \mathbf{B} in the CORREL run have not been optimized. For instance, nothing tells us that the correlations have a Gaussian shape neither that the length scales are 600 km horizontally at every model level or 1 level vertically. In principle, a calibrated \mathbf{B} should improve the analyses. Several methods have been developed by the NWP centers and are reviewed by Bannister (2008a, Sect. 5). This optimization effort has not been implemented in the present study. Indeed, we aimed to focus on the implementations of the correlations and not essentially on the BASCOE results. We nevertheless plan to present the optimization of the parameters of \mathbf{B} in future papers.

7 Conclusions

There are several outcomes from this work. First, we have gathered together all the material published so far in order to provide a stand alone document describing the

Spectral representation of background error covariances

Q. Errera and R. Ménard

Title Page

Abstract

Introduction

Conclusions

References

Tables

Figures

⏪

⏩

◀

▶

Back

Close

Full Screen / Esc

Printer-friendly Version

Interactive Discussion



spherical harmonic representation of the background error covariance matrix (the **B** matrix) in the case of univariate assimilation. The motivation of a spherical harmonic representation of **B** is based on the fact that, if horizontal correlations are assumed homogeneous and isotropic, **B** can be represented in the spectral space by a block diagonal matrix with repeated matrices for each zonal wavenumber m , which makes its numerical computation feasible. Horizontal and vertical correlations can be implemented in two ways. The first one consists in providing correlation functions for the vertical and the horizontal directions (not necessarily the same) along with correlation length scales. In the second method, these correlation matrices are calibrated using optimization methods such as those summarized by Bannister (2008a, Sect. 5). This later method allows the implementation of non-separable spatial correlations. This has proved to be important in meteorology but has never been studied in chemistry.

The second outcome of this study is to provide the numerical Fortran code of the formulation of the **B** matrix (see the Supplement of this paper). During the course of this implementation, we realized that only the adjoint of the spectral transform operator was necessary for variational assimilation, not the inverse. The problem with the inverse operator is to restrict the target grid of the spectral transform to the (non-equally spaced) Gaussian grid. On the other hand, the adjoint operator does not suffer this limitation thus allowing the use of the (equally spaced) model grid. In this way, there is no need to implement a grid transformation from the Gaussian grid to the lat/lon (model) grid which degrades the analyses.

The spherical harmonic representation of **B** has been implemented in the 4D-Var stratospheric chemical assimilation system BASCOE using the Michelson Interferometer for Passive Atmosphere Sounding (MIPAS) ozone observations between August and October 2003. Two experiments were performed: the one considering a spectral formulation of **B** and the other considering the diagonal **B** (i.e. spatially uncorrelated) implemented so far in BASCOE. In those experiments, the chemical and PSC schemes of BASCOE were turned off such that the influence of ozone observations on other modeled constituents has not been studied. At southern high latitudes and

Spectral representation of background error covariances

Q. Errera and R. M enard

Title Page

Abstract

Introduction

Conclusions

References

Tables

Figures

◀

▶

◀

▶

Back

Close

Full Screen / Esc

Printer-friendly Version

Interactive Discussion



during the ozone hole, the spatially correlated **B** allows a great improvement of the analyses with respect to the uncorrelated one. The correlations allow to increase the size of the analysis increments which allow to produce ozone fields in good agreement against ozonesondes and total ozone observations, which is not the case for the analyses calculated with the diagonal **B**.

In the future, two studies are planned. The first one is to adapt this formulation for BASCOE in the case where the chemistry module is turned on and to evaluate the improvements to constituents other than ozone. The second study consists in estimating the correlation matrices by one of the method reviewed by Bannister (2008a, Sect. 5) for separable and non-separable spatial correlations. In the atmosphere, the constituent's concentrations can vary with height by several orders of magnitude and chemical regimes can completely change with altitude, for instance across the tropopause and stratopause. For those reasons, the horizontal and vertical lengths scales are likely to be strongly dependent on height. Thus a non-separable three-dimensional error correlation matrix could provide a better representation of the background error for chemical variables than a separable matrix.

Appendix A

Complement on spherical harmonic representation

A1 Normalization of spherical harmonics

Let us recall the definition of the spherical harmonics:

$$Y_n^m(\lambda, \mu) = N_n^m P_n^m(\mu) e^{im\lambda} \quad (\text{A1})$$

where

$$P_n^m(\mu) = \frac{(1-\mu^2)^{m/2}}{2^n n!} \frac{d^{n+m}}{d\mu^{n+m}} (\mu^2 - 1)^n \quad (\text{A2})$$

are the associated Legendre functions. Since

$$\int_0^{2\pi} e^{i(m-m')\lambda} d\lambda = 2\pi \delta_m^{m'} \quad (\text{A3})$$

5 and

$$\int_{-1}^1 P_n^m(\mu) P_{n'}^m(\mu) d\mu = \left(\frac{2}{2n+1} \right) \left[\frac{(n+m)!}{(n-m)!} \right] \delta_n^{n'}, \quad (\text{A4})$$

(where we note that associated Legendre functions are not orthogonal for different value of m), we have

$$\int_{-\pi}^{\pi} \int_{-1}^1 Y_n^m(\lambda, \mu) (Y_{n'}^{m'}(\lambda, \mu))^* d\mu d\lambda = \left(\frac{4\pi}{2n+1} \right) \left[\frac{(n+m)!}{(n-m)!} \right] (N_n^m)^2 \delta_n^{n'} \delta_m^{m'}. \quad (\text{A5})$$

10 The normalization constants N_n^m take a different form following the choice of inner-product of the spherical harmonics. For practical reasons, there are several ways to

Spectral representation of background error covariances

Q. Errera and R. Ménard

Title Page

Abstract

Introduction

Conclusions

References

Tables

Figures

⏪

⏩

◀

▶

Back

Close

Full Screen / Esc

Printer-friendly Version

Interactive Discussion



normalize the spherical harmonics

$$\int_{\Omega} Y_n^m(\Omega) Y_{n'}^{m'}(\Omega) d\Omega = \begin{cases} \frac{4\pi}{2n+1} \frac{(n+m)!}{(n-m)!} \delta_n^{n'} \delta_m^{m'} & \text{UN} \\ \frac{4\pi}{2n+1} \delta_n^{n'} \delta_m^{m'} & \text{Schmit} \\ \delta_n^{n'} \delta_m^{m'} & \text{ON} \\ 4\pi \delta_n^{n'} \delta_m^{m'} & \text{G4}\pi \\ 2\pi \delta_n^{n'} \delta_m^{m'} & \text{G2}\pi \end{cases} \quad (\text{A6})$$

where the abbreviations have the following meaning: UN for *unnormalized*, Schmit for *Schmit semi-normalized*, ON for *orthonormalized*, G4 π for *geodesy 4 π* (as in Courtier et al., 1998) and G2 π for *geodesy 2 π* (as in this paper and in Boer, 1983). These different normalizations of the spherical harmonics define the value of the normalization constant:

$$N_n^m = \begin{cases} 1 & \text{UN} \\ \left[\frac{(n-m)!}{(n+m)!} \right]^{1/2} & \text{Schmit} \\ \left(\frac{2n+1}{4\pi} \right)^{1/2} \left[\frac{(n-m)!}{(n+m)!} \right]^{1/2} & \text{ON} \\ \sqrt{2n+1} \left[\frac{(n-m)!}{(n+m)!} \right]^{1/2} & \text{G4}\pi \\ \left(\frac{2n+1}{2} \right)^{1/2} \left[\frac{(n-m)!}{(n+m)!} \right]^{1/2} & \text{G2}\pi \end{cases} \quad (\text{A7})$$

For practical reasons, computer code implementations often introduced the normalization factor into the associated Legendre functions (which is done in the code provided in the Supplement). In this case, we define the normalized associated Legendre functions: $\bar{P}_n^m(\mu) = N_n^m P_n^m(\mu)$. Accordingly, the computation of spherical harmonics is decomposed into the product of two functions or two operations, a Fourier term and

Spectral representation of background error covariances

Q. Errera and R. Ménard

Title Page

Abstract

Introduction

Conclusions

References

Tables

Figures

⏪

⏩

◀

▶

Back

Close

Full Screen / Esc

Printer-friendly Version

Interactive Discussion



a Legendre term. For the normalized associated Legendre functions, we have

$$\int_{-1}^1 \bar{P}_n^m(\mu) \bar{P}_{n'}^m(\mu) d\mu = \begin{cases} \frac{2}{2n+1} \frac{(n-m)!}{(n+m)!} \delta_n^{n'} & \text{UN} \\ \frac{2}{2n+1} \delta_n^{n'} & \text{Schmit} \\ \frac{1}{2\pi} \delta_n^{n'} & \text{ON} \\ 2\delta_n^{n'} & \text{G4}\pi \\ \delta_n^{n'} & \text{G2}\pi \end{cases} \quad (\text{A8})$$

One easy way to check the choice of normalization is to verify that $\bar{P}_n^0(\mu = 0) = N_n^0$, i.e.

$$\bar{P}_n^0(0) = \begin{cases} 1 & \text{UN} \\ 1 & \text{Schmit} \\ \left(\frac{2n+1}{4\pi}\right)^{1/2} & \text{ON} \\ \sqrt{2n+1} & \text{G4}\pi \\ \left(\frac{2n+1}{2}\right)^{1/2} & \text{G2}\pi \end{cases} \quad (\text{A9})$$

However, note that this check does not make any difference between UN and Schmit normalization.

Finally, let us mention the following property $\bar{P}_n^{-m} = (-1)^m \bar{P}_n^m$ (which is not valid for unnormalized associated Legendre functions). It follows that $(Y_n^m)^* = (-1)^m Y_n^{-m}$.

A2 Inverse of spectral transform from non-Gaussian grid

It is worth noting that the inverse transform on other grids than the Gaussian grid can be made by a quadrature developed by Machenhauer and Daley (1972), which has the same numerical accuracy (although not exact) as the method based on the Gaussian

grid (see also Swarztrauber, 1979; Machenhauer, 1979, Sect. 4.6):

$$\Psi_n^m = \frac{1}{M} \sum_{k=1}^K \sum_{j=0}^{M-1} \Psi_n^m(\lambda_j, \mu_k) Z_n^m(\mu_k) e^{-im\lambda_j} \quad (\text{A10})$$

$$Z_n^m(\mu_k) = \frac{1}{K} \sum_{r=0}^N \delta L_r(\mu_k) \int_{-1}^1 L_r(\mu) \bar{P}_n^m(\mu) d\mu \quad (\text{A11})$$

$$\delta = \begin{cases} 1/2 & \text{for } r = 0 \\ 1 & \text{for } r \neq 0 \end{cases} \quad (\text{A12})$$

and

$$L_r(\mu) = \begin{cases} \cos(r\mu) & \begin{cases} m \text{ and } r \text{ odd} \\ m \text{ and } r \text{ even} \end{cases} \\ \sin(r\mu) & \begin{cases} m \text{ even and } r \text{ odd} \\ m \text{ odd and } r \text{ even} \end{cases} \end{cases} \quad (\text{A13})$$

The integral on the right-hand side in Eq. (A11) can be computed exactly by a Gaussian quadrature.

The code available in the Supplement provides the routine to calculate the inverse operation \mathbf{S}^{-1} from the Gaussian grid (but not from the equally spaced lat/lon grid). Such a routine can be found in the SPHEREPACK module available at www2.cisl.ucar.edu/resources/legacy/spherepack.

A3 Addition theorem of spherical harmonics

The derivation of the spectral representation of homogeneous and isotropic horizontal correlations requires the use of the addition theorem of spherical harmonics. Suppose

Spectral representation of background error covariances

Q. Errera and R. Ménard

Title Page

Abstract

Introduction

Conclusions

References

Tables

Figures

⏪

⏩

◀

▶

Back

Close

Full Screen / Esc

Printer-friendly Version

Interactive Discussion



we have two points on a unit sphere $\Omega = (\lambda, \mu)$ and $\Omega' = (\lambda', \mu')$. Let θ denote the great circle angular separation between those points which is defined by

$$\cos \theta = \sin \mu \sin \mu' + \cos \mu \cos \mu' \cos(\lambda' - \lambda). \quad (\text{A14})$$

The addition theorem of spherical harmonics state that (Jackson, 1998):

$$\sum_{m=-n}^n Y_n^m(\Omega) (Y_n^m(\Omega'))^* = (N_n^0)^2 P_n(\cos \theta) \quad (\text{A15})$$

or

$$\sum_{m=-n}^n Y_n^m(\Omega) (Y_n^m(\Omega'))^* = (N_n^0) \bar{P}_n(\cos \theta). \quad (\text{A16})$$

A4 Homogeneous and isotropic horizontal correlations

Let $\epsilon(\Omega)$ be a 2-D error field on the sphere as defined in Sect. 2.6 and ϵ_n^m its spectral coefficients. The physical representation of the correlations $\langle \epsilon(\Omega)\epsilon(\Omega') \rangle$ and its spectral counterpart $\langle \epsilon_n^m \epsilon_{n'}^{m'} \rangle$ are related by

$$\langle \epsilon(\Omega)\epsilon(\Omega') \rangle = \sum_{n=0}^N \sum_{m=-n}^n \sum_{n'=0}^N \sum_{m'=-n'}^{n'} \langle \epsilon_n^m \epsilon_{n'}^{m'} \rangle Y_n^m(\Omega) (Y_{n'}^{m'}(\Omega'))^* \quad (\text{A17})$$

and by the inverse relationship

$$\langle \epsilon_n^m \epsilon_{n'}^{m'} \rangle = \frac{1}{4\pi^2} \int_{\Omega} \int_{\Omega'} \langle \epsilon(\Omega)\epsilon(\Omega') \rangle Y_n^m(\Omega) (Y_{n'}^{m'}(\Omega'))^* d\Omega d\Omega'. \quad (\text{A18})$$

Spectral representation of background error covariances

Q. Errera and R. Ménard

Title Page

Abstract

Introduction

Conclusions

References

Tables

Figures

◀

▶

◀

▶

Back

Close

Full Screen / Esc

Printer-friendly Version

Interactive Discussion



Assuming homogeneous and isotropic covariances using Eq. (21), Eq. (A18) can be rewritten as

$$\langle \epsilon_n^m \epsilon_{n'}^{m'} \rangle = \frac{1}{4\pi^2} \sum_{n''} f_{n''} \int_{\Omega} \int_{\Omega'} \bar{P}_{n''}(\cos \theta) Y_n^m(\Omega) (Y_{n'}^{m'}(\Omega'))^* \mathbf{d}\Omega \mathbf{d}\Omega' . \quad (\text{A19})$$

5 Using the addition theorem of spherical harmonics, Eq. (A19) becomes

$$\langle \epsilon_n^m \epsilon_{n'}^{m'} \rangle = \frac{1}{4\pi^2} \sum_{n''} f_{n''} (N_{n''}^0)^{-1} \int_{\Omega} \int_{\Omega'} Y_n^m(\Omega) \sum_{m''=-n''}^{n''} (Y_{n''}^{m''}(\Omega))^* Y_{n''}^{m''}(\Omega') (Y_{n'}^{m'}(\Omega'))^* \mathbf{d}\Omega \mathbf{d}\Omega' \quad (\text{A20})$$

which yields

$$\langle \epsilon_n^m \epsilon_{n'}^{m'} \rangle = b_n \delta_n^m \delta_{n'}^{m'} ; \quad b_n \equiv f_n / N_n \quad (\text{A21})$$

10 as a result of the orthogonality of the spherical harmonics. Equation (A21) is a necessary condition when correlations are homogeneous and isotropic. By substituting Eq. (A21) in (A17) and using the addition theorem of spherical harmonics, one finds Eq. (21), thus proving that Eq. (A21) is also sufficient.

Let us see how this result is extended in three dimensions. Let $\zeta(\Omega, \rho)$ be a 3-D error field on the sphere where ρ denotes the altitude. Again, we assume that ζ is unbiased and normalized such that $\langle \zeta(\Omega, \rho)^2 \rangle = 1$. Equation (A21) obtained in two dimensions is generalized in three dimensions as follows:

$$\langle \zeta_n^m \zeta_{n'}^{m'} \rangle = \sqrt{b_n(\rho) b_{n'}(\rho')} \mathbf{C}_n^v(\rho, \rho') \delta_n^m \delta_{n'}^{m'} . \quad (\text{A22})$$

20 where \mathbf{C}_n^v is the vertical correlation matrix for the wavenumber n and the coefficients b_n are now dependent on the altitude.

Spectral representation of background error covariances

Q. Errera and R. Ménard

Title Page

Abstract

Introduction

Conclusions

References

Tables

Figures

⏪

⏩

◀

▶

Back

Close

Full Screen / Esc

Printer-friendly Version

Interactive Discussion



Spectral representation of background error covariances

Q. Errera and R. Ménard

Title Page

Abstract

Introduction

Conclusions

References

Tables

Figures

⏪

⏩

◀

▶

Back

Close

Full Screen / Esc

Printer-friendly Version

Interactive Discussion



If \mathbf{C}_n^v and $b_n(p)$ are independent of n and p , respectively, (A22) might be rewritten as

$$\langle \xi_n^m p \xi_{n'}^{m'} p' \rangle = b_n \mathbf{C}^v(p, p') \delta_n^{n'} \delta_m^{m'} \tag{A23}$$

and we can prove that the spatial correlations are separable. By definition, a matrix is said separable if it can be calculated by a tensor product of two sub-matrices. In this case, if the horizontal and vertical correlation matrices are denoted by \mathbf{C}^h and \mathbf{C}^v , then the 3-D spatial correlation matrix \mathbf{C} is defined by

$$\mathbf{C} = \mathbf{C}^h \otimes \mathbf{C}^v \tag{A24}$$

where \otimes denotes the Kronecker tensor product. In terms of matrix elements, and considering homogeneous and isotropic correlations, we have

$$C(\Omega, p, \Omega', p') = f(\theta) C^v(p, p') . \tag{A25}$$

Indeed, the correlations in the physical space might have the following spectral representation

$$\langle \xi(\Omega, p) \xi(\Omega', p') \rangle = \sum_{n=0}^N \sum_{m=-n}^n \sum_{n'=0}^N \sum_{m'=-n'}^{n'} \langle \xi_n^m p \xi_{n'}^{m'} p' \rangle Y_n^m(\Omega) (Y_{n'}^{m'}(\Omega'))^* . \tag{A26}$$

By using Eq. (A23), Eq. (A26) takes the form

$$\langle \xi(\Omega, p) \xi(\Omega', p') \rangle = C^v(p, p') \sum_{n=0}^N \sum_{m=-n}^n b_n Y_n^m(\Omega) (Y_n^m(\Omega'))^* . \tag{A27}$$

and using the Eq. (A16), the previous equation can be rewritten as

$$\langle \xi(\Omega, p) \xi(\Omega', p') \rangle = C^v(p, p') \sum_{n=0}^N N_n b_n \bar{P}_n(\cos \theta) \tag{A28}$$

5

10

15

20

which leads to Eq. (A25). If spatial correlations are separable, Eq. (A28) is a necessary condition. To prove that the condition is sufficient, we substitute Eq. (A28) in

$$\langle \zeta_n^m p \zeta_{n'}^{m'} p' \rangle = \frac{1}{4\pi^2} \int \int_{\Omega \Omega'} \langle \zeta(\Omega, p) \zeta(\Omega', p') \rangle Y_n^m(\Omega) (Y_{n'}^{m'}(\Omega'))^* d\Omega d\Omega' . \quad (\text{A29})$$

5 and using the orthogonality of the spherical harmonics and the addition theorem, we can find Eq. (A23).

Appendix B

Fortran code

10 The Supplement of this paper provides a code that allows calculation of the operations \mathbf{L} and \mathbf{L}^* along with two test programs. The operations related to the \mathbf{B} matrix are given in `bglib.sh.f90` (which means “BackGround LIBrary and Spherical Harmonics representation”). The length of this file is rather short. Moreover, we tried to use Fortran variable names that are close to those presented here. The correspondence between the different operators discussed in Sect. 3 and their coded
 15 counterpart are given in Table 2. A very important routine is `PRECOMPUTE_BGLIB` which precomputes values used by the different operators. They are described in Table 3. The Gaussian latitudes and weights such as the associated Legendre functions are precalculated by the freely available software `SHTOOLS` (available at: <http://www.ipgp.fr/~wieczor/SHTOOLS/SHTOOLS.html>) which needs to be installed before
 20 compiling the code. The vertical correlation matrix is calculated during the precomputing and its square root is calculated using singular value decomposition (SVD). The SVD uses LAPACK libraries which also need to be installed.

In order to allow the user to check if this code fulfills his needs without having to install the `SHTOOLS` library or LAPACK (while this later is usually installed), this code can

Spectral representation of background error covariances

Q. Errera and R. Ménard

Title Page

Abstract

Introduction

Conclusions

References

Tables

Figures



Back

Close

Full Screen / Esc

Printer-friendly Version

Interactive Discussion



also be compiled in a “demo” mode. In this case, the Gaussian latitudes and weights, the associated Legendre functions and the vertical correlation matrix are read in files also provided. However, this mode is only available for a size grid of $120 \times 60 \times 31$ in lon/lat/lev as for vertical Gaussian correlations with $L_v = 3$ levels.

In addition to the library of the spectral representation of \mathbf{B} , the code is provided with two tests. The first one checks that the test of the adjoint is satisfied, i.e. $\langle \mathbf{x}, \mathbf{L}\chi \rangle = \langle \mathbf{L}^* \mathbf{x}, \chi \rangle$ for any value of \mathbf{x} and χ . This is the case if we exclude round-off errors. This test is calculated by `test_adj.f90`. The second test is the assimilation of a single pseudo-observation as presented in Sect. 5. For this test, a simulator is given (`simul_sh.f90`) and the quasi-Newton minimizer M1QN3 (`m1qn3.f90`, Gilbert and Lemarechal, 1989).

Information necessary to compile and run the code, and the conditions for its use, are provided in a README file given in the Supplement.

In terms of numerical performances, this code is very low demanding in computer resources (CPU and memory). On a single processor, the CPU time consumed by the operations \mathbf{L} and \mathbf{L}^* is lower than the time consumed by M1QN3. For the real assimilation test case as discussed in the Sect. 6, the operations \mathbf{L} and \mathbf{L}^* take less than 1 % of the total CPU time. On an AMD Opteron 1.15 GHz processor and considering a model resolution of $180 \times 91 \times 37$ grid points, the total time necessary to calculate the operations \mathbf{L} and \mathbf{L}^* is ~ 1.1 s (~ 0.55 s each).

Supplementary material related to this article is available online at:
<http://www.atmos-chem-phys-discuss.net/12/16763/2012/acpd-12-16763-2012-supplement.zip>.

Acknowledgements. We wish to thank Mark Wieczorek for making SHTOOLS available and Mark Buehner and Pierre Gautier for their help in the implementation of, respectively, the adjoint operator \mathbf{S}^* and the calculation of the spectral correlation coefficients. QE is supported by Belgian Science Policy (BELSPO) Prodex program under the project A3C. Part of the data

Spectral representation of background error covariances

Q. Errera and R. Ménard

Title Page

Abstract

Introduction

Conclusions

References

Tables

Figures

⏪

⏩

◀

▶

Back

Close

Full Screen / Esc

Printer-friendly Version

Interactive Discussion

used in this publication were obtained as part of the Network for the Detection of Atmospheric Composition Change (NDACC) and are publicly available (see <http://www.ndacc.org>).

References

- 5 Bannister, R. N.: A review of forecast error covariance statistics in atmospheric variational data assimilation. I: characteristics and measurements of forecast error covariances, *Q. J. R. Meteorol. Soc.*, 134, 1951–1970, 2008a. 16776, 16780, 16785, 16786, 16787
- Bannister, R. N.: A review of forecast error covariance statistics in atmospheric variational data assimilation. II: modelling the forecast error covariance statistics, *Q. J. R. Meteorol. Soc.*, 134, 1971–1996, 2008b. 16776
- 10 Bartello, P. and Mitchell, H. L.: A continuous three-dimensional model of short-range forecast error covariances, *Tellus A*, 44, 217, doi:10.1034/j.1600-0870.1992.t01-2-00002.x, 1992. 16779
- Berre, L.: Estimation of synoptic and mesoscale forecast error covariances in a limited-area model, *Mon. Weather Rev.*, 128, 644, doi:10.1175/1520-0493(2000)128<0644:EOSAMF>2.0.CO;2, 2000. 16779
- 15 Boer, G. J.: Homogeneous and isotropic turbulence on the sphere, *J. Atmos. Sci.*, 40, 154–163, 1983. 16765, 16774, 16789
- Boer, G. J. and Shepherd, T. G.: Large-scale two-dimensional turbulence in the atmosphere, *J. Atmos. Sci.*, 40, 164–184, 1983. 16765
- 20 Cortesi, U., Lambert, J. C., De Clercq, C., Bianchini, G., Blumenstock, T., Bracher, A., Castelli, E., Catoire, V., Chance, K. V., De Mazière, M., Demoulin, P., Godin-Beekmann, S., Jones, N., Jucks, K., Keim, C., Kerzenmacher, T., Kuellmann, H., Kuttippurath, J., Iarlori, M., Liu, G. Y., Liu, Y., McDermid, I. S., Meijer, Y. J., Mencaraglia, F., Mikuteit, S., Oelhaf, H., Piccolo, C., Pirre, M., Raspollini, P., Ravegnani, F., Reburn, W. J., Redaelli, G., Remedios, J. J., Sembhi, H., Smale, D., Steck, T., Taddei, A., Varotsos, C., Vigouroux, C., Waterfall, A., Wetzel, G., and Wood, S.: Geophysical validation of MIPAS-ENVISAT operational ozone data, *Atmos. Chem. Phys.*, 7, 4807–4867, doi:10.5194/acp-7-4807-2007, 2007. 16785
- 25 Courtier, P., Andersson, E., Heckley, W., Vasiljevic, D., Hamrud, M., Hollingsworth, A., Rabier, F., Fisher, M., and Pailleux, J.: The ECMWF implementation of three-dimensional

Spectral representation of background error covariances

Q. Errera and R. Ménard

Title Page

Abstract

Introduction

Conclusions

References

Tables

Figures

⏪

⏩

◀

▶

Back

Close

Full Screen / Esc

Printer-friendly Version

Interactive Discussion



Spectral representation of background error covariances

Q. Errera and R. Ménard

Title Page

Abstract

Introduction

Conclusions

References

Tables

Figures

⏪

⏩

◀

▶

Back

Close

Full Screen / Esc

Printer-friendly Version

Interactive Discussion

variational assimilation (3D-Var). I: formulation, Q. J. R. Meteorol. Soc., 124, 1783–1807, doi:10.1002/qj.49712455002, 1998. 16765, 16767, 16776, 16778, 16789

Dee, D. P.: On-line estimation of error covariance parameters for atmospheric data assimilation, Mon. Weather Rev., 123, 1128, doi:10.1175/1520-0493(1995)123<1128:OLEOEC>2.0.CO;2, 1995. 16776

Dee, D. P., Uppala, S. M., Simmons, A. J., Berrisford, P., Poli, P., Kobayashi, S., Andrae, U., Balmaseda, M. A., Balsamo, G., Bauer, P., Bechtold, P., Beljaars, A. C. M., van de Berg, L., Bidlot, J., Bormann, N., Delsol, C., Dragani, R., Fuentes, M., Geer, A. J., Haimberger, L., Healy, S. B., Hersbach, H., Hólm, E. V., Isaksen, I., Kållberg, P., Köhler, M., Matricardi, M., McNally, A. P., Monge-Sanz, B. M., Morcrette, J.-J., Park, B.-K., Peubey, C., de Rosnay, P., Tavolato, C., Thépaut, J.-N., and Vitart, F.: The ERA-Interim reanalysis: configuration and performance of the data assimilation system, Q. J. R. Meteorol. Soc., 137, 553–597, doi:10.1002/qj.828, 2011. 16784

Derber, J. and Rosati, A.: A global oceanic data assimilation system, J. Phys. Oceanogr., 19, 1333–1347, doi:10.1175/1520-0485(1989)019<1333:AGODAS>2.0.CO;2, 1989. 16765

Dethof, A. and Hólm, E. V.: Ozone assimilation in the ERA-40 reanalysis project, Q. J. R. Meteorol. Soc., 130, 2851–2872, doi:10.1256/qj.03.196, 2004. 16765

Elbern, H., Schwinger, J., and Botchorishvili, R.: Chemical state estimation for the middle atmosphere by four-dimensional variational data assimilation: system configuration, J. Geophys. Res., 115, D06302, doi:10.1029/2009JD011953, 2010. 16765

Errera, Q., Daerden, F., Chabrillat, S., Lambert, J. C., Lahoz, W. A., Viscardy, S., Bonjean, S., and Fonteyn, D.: 4D-Var assimilation of MIPAS chemical observations: ozone and nitrogen dioxide analyses, Atmos. Chem. Phys., 8, 6169–6187, doi:10.5194/acp-8-6169-2008, 2008. 16783, 16784

Fischer, H., Birk, M., Blom, C., Carli, B., Carlotti, M., von Clarmann, T., Delbouille, L., Dudhia, A., Ehhalt, D., Endemann, M., Flaud, J. M., Gessner, R., Kleinert, A., Koopman, R., Langen, J., López-Puertas, M., Mosner, P., Nett, H., Oelhaf, H., Perron, G., Remedios, J., Ridolfi, M., Stiller, G., and Zander, R.: MIPAS: an instrument for atmospheric and climate research, Atmos. Chem. Phys., 8, 2151–2188, doi:10.5194/acp-8-2151-2008, 2008. 16784

Fisher, M.: Background error covariance modelling, in: Seminar on Recent developments in data assimilation for atmosphere and ocean, 8–12 September 2003, edited by: ECMWF, Shinfield Park, Reading, 45–64, 2003. 16765, 16779

Spectral representation of background error covariances

Q. Errera and R. Ménard

Title Page

Abstract

Introduction

Conclusions

References

Tables

Figures

⏪

⏩

◀

▶

Back

Close

Full Screen / Esc

Printer-friendly Version

Interactive Discussion



- Gaspari, G. and Cohn, S. E.: Construction of correlation functions in two and three dimensions, *Q. J. R. Meteorol. Soc.*, 125, 723–757, 1999. 16773
- Gauthier, P., Courtier, P., and Moll, P.: Assimilation of simulated wind lidar data with a Kalman filter, *Mon. Weather Rev.*, 121, 1803, doi:10.1175/1520-0493(1993)121<1803:AOSWLD>2.0.CO;2, 1993. 16774
- 5 Geer, A. J., Lahoz, W. A., Bekki, S., Bormann, N., Errera, Q., Eskes, H. J., Fonteyn, D., Jackson, D. R., Juckes, M. N., Massart, S., Peuch, V.-H., Rharmili, S., and Segers, A.: The ASSET intercomparison of ozone analyses: method and first results, *Atmos. Chem. Phys.*, 6, 5445–5474, doi:10.5194/acp-6-5445-2006, 2006. 16783, 16784
- 10 Gilbert, J.-C. and Lemarechal, C.: Some numerical experiments with variable storage quasi-Newton algorithms, *Math. Prog.*, 45, 407–435, 1989. 16781, 16796
- Jackson, J. D.: *Classical Electrodynamics*, 3rd edn., Wiley & Sons, 1998. 16792
- Krishnamurti, T. N., Bedi, H. S., Hardiker, V. M., and Ramaswamy, L.: *An Introduction to Global Spectral Modeling*, 2nd revised and enlarged edition, Springer, 2006. 16767, 16770, 16772
- 15 Lahoz, W. A., Errera, Q., Viscardy, S., and Manney, G. L.: The 2009 stratospheric major warming described from synergistic use of BASCOE water vapour analyses and MLS observations, *Atmos. Chem. Phys.*, 11, 4689–4703, doi:10.5194/acp-11-4689-2011, 2011. 16783
- Lin, S.-J. and Rood, R. B.: Multidimensional flux-form semi-Lagrangian transport schemes, *Mon. Weather Rev.*, 124, 2046–2070, 1996. 16783
- 20 Machenhauer, B.: The spectral method, in: *Numerical Methods used in Atmospheric Models*, edited by: Kasahara, E. A., No. 17 in GARP Publication Series, WMO, 1979. 16791
- Machenhauer, B. and Daley, R.: A baroclinic primitive equation model with a spectral representation in three dimensions, *Tech. Rep. 4*, Institute for Theoretical Meteorology, Copenhagen University, 1972. 16790
- 25 Monin, A. S. and Yaglom, A. M.: *Statistical Fluid Mechanics: Mechanics of Turbulence*, vol. 1, The MIT Press, 1971. 16765
- Monin, A. S. and Yaglom, A. M.: *Statistical Fluid Mechanics: Mechanics of Turbulence*, vol. 2, The MIT Press, 1975. 16765
- Panchev, S.: *Random Functions and Turbulence*, International Series of Monograph in Natural Philosophy, Pergamon Press, 1971. 16765
- 30 Parrish, D. F. and Derber, J. C.: The National Meteorological Center's spectral statistical-interpolation analysis system, *Mon. Weather Rev.*, 120, 1747–1763, 1992. 16764

Spectral representation of background error covariances

Q. Errera and R. Ménard

Title Page

Abstract

Introduction

Conclusions

References

Tables

Figures

⏪

⏩

◀

▶

Back

Close

Full Screen / Esc

Printer-friendly Version

Interactive Discussion



- Phillips, N. A.: The spatial statistics of random geostrophic modes and first-guess errors, *Tellus A*, 38, 314, doi:10.1111/j.1600-0870.1986.tb00418.x, 1986. 16779
- Satoh, M.: *Atmospheric Circulation Dynamics and Circulation Models*, Springer, 2004. 16767, 16770
- 5 Schwinger, J. and Elbern, H.: Chemical state estimation for the middle atmosphere by four-dimensional variational data assimilation: a posteriori validation of error statistics in observation space, *J. Geophys. Res.*, 115, D18307, doi:10.1029/2009JD013115, 2010. 16765
- Swarztrauber, P. N.: On the spectral approximation of discrete scalar and vector functions on the sphere, *SIAM J. Numer. Anal.*, 16, 934–949, doi:10.1137/0716069, 1979. 16791
- 10 Swarztrauber, P. N.: Discrete Fourier transforms and related topics, available at: <http://www.cisl.ucar.edu/css/staff/pauls/tutorials/index.html>, Lecture 1. 16772
- Swarztrauber, P. N.: Computing on the sphere: Part I, available at: <http://www.cisl.ucar.edu/css/staff/pauls/tutorials/index.html>, Lecture 2. 16772
- Talagrand, O.: Assimilation of observations, an introduction, *J. Meteorol. Soc. Jpn*, 277, 191–209, 1997. 16774
- 15 Viscardy, S., Errera, Q., Christophe, Y., Chabrilat, S., and Lambert, J.-C.: Evaluation of ozone analyses from UARS MLS assimilation by BASCOE between 1992 and 1997, *JSTARS*, 3, 190–202, doi:10.1109/JSTARS.2010.2040463, 2010. 16783
- Weaver, A. and Courtier, P.: Correlation modelling on the sphere using a generalized diffusion equation, *Q. J. R. Meteorol. Soc.*, 127, 1815–1846, doi:10.1002/qj.49712757518, 2001. 16765
- 20

Spectral representation of background error covariances

Q. Errera and R. M enard

Title Page

Abstract

Introduction

Conclusions

References

Tables

Figures

◀

▶

◀

▶

Back

Close

Full Screen / Esc

Printer-friendly Version

Interactive Discussion



Table 1. Scores of the single-observation assimilation using two different spectral grids: the model lat/lon grid and the Gaussian grid. We report the value of the objective function J for the analysis, the analysis at the observation location $H(\mathbf{x})$, the analysis correlation length scales obtained by fitting the analysis cross-sections (see Fig. 1) by a Gaussian function, and the root mean square (RMS) between the analysis and the expected Gaussian function.

	Expected value	Lat/Lon Grid	Gaussian Grid
J	1.0	1.0038	1.0416
$H(\mathbf{x})$	1.1	1.101	1.0966
L_h^{lat}	600	576	622
L_h^{lon}	600	576	573.8
L_v	3	2.88	2.87
RMS_{lat}	0	7.82×10^{-7}	8.3×10^{-3}
RMS_{lon}	0	3.06×10^{-5}	1.2×10^{-4}
RMS_{lev}	0	5.37×10^{-5}	2.1×10^{-4}

Spectral representation of background error covariances

Q. Errera and R. Ménard

Title Page

Abstract

Introduction

Conclusions

References

Tables

Figures

⏪

⏩

◀

▶

Back

Close

Full Screen / Esc

Printer-friendly Version

Interactive Discussion

Table 2. List of operators and matrix operations that define \mathbf{L} and \mathbf{L}^* , and the routines in which they are coded.

Operator	corresponding routine
\mathbf{S}	S_DIRECT
\mathbf{S}^*	S_ADJ
\mathbf{S}^{-1}	S_INV ^a
$\mathbf{\Lambda}^{1/2}$	SQRT_CORREL
\mathbf{G}	SG2MG
\mathbf{G}^T	AD_SG2MG
$\mathbf{\Sigma}$	B_STDDEV

^a \mathbf{S}^{-1} is only coded for the transform from the Gaussian grid to the spectral space.

Spectral representation of background error covariances

Q. Errera and R. Ménard

Title Page

Abstract

Introduction

Conclusions

References

Tables

Figures

⏪

⏩

◀

▶

Back

Close

Full Screen / Esc

Printer-friendly Version

Interactive Discussion

Table 3. List of precalculated variables and their Fortran counterpart.

Variable names	corresponding Fortran names
μ	mu
λ	lambda
w	wg
P_n^m	Pnm
$e^{im\lambda}$	Eiml
\mathbf{G}	G
\mathbf{G}^T	G_TRANSP
$(\mathbf{C}^v)^{1/2}$	Cv
b_n	Values stored in Ch
Σ	bg_std

Spectral representation of background error covariances

Q. Errera and R. Ménard

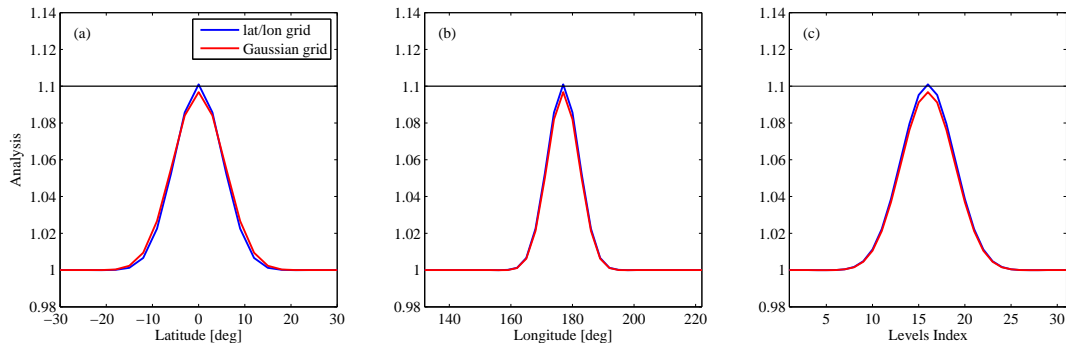


Fig. 1. Cross-sections of the analyses obtained by the assimilation of a single pseudo-observations using Gaussian spatial correlation function and two spectral grids: the lat/lon grid (blue line) and the Gaussian grid (red line). The correlation length scales are $L_h = 600$ km horizontally and $L_v = 3$ model levels vertically. The three panels show the cross-section of these analyses along the latitude **(a)**, the longitude **(b)** and the altitude **(c)**, all crossing the observation location. The horizontal black lines at value 1.1 indicate the theoretical analyses at the observation location.

Title Page

Abstract

Introduction

Conclusions

References

Tables

Figures

◀

▶

◀

▶

Back

Close

Full Screen / Esc

Printer-friendly Version

Interactive Discussion



Spectral representation of background error covariances

Q. Errera and R. Ménard

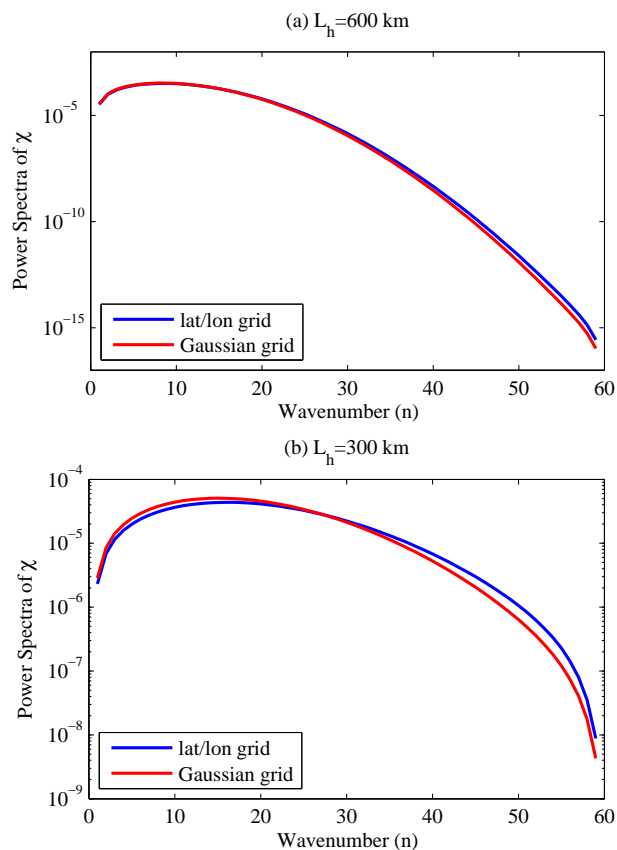


Fig. 2. Power spectra of the analysis increments χ at the observation level obtained using two different spectral grids – the lat/lon grid (blue line) and the Gaussian grid (red line) – and two correlation length scales – $L_h = 600$ km **(a)** and 300 km **(b)**.

[Title Page](#)[Abstract](#)[Introduction](#)[Conclusions](#)[References](#)[Tables](#)[Figures](#)[◀](#)[▶](#)[◀](#)[▶](#)[Back](#)[Close](#)[Full Screen / Esc](#)[Printer-friendly Version](#)[Interactive Discussion](#)

Spectral representation of background error covariances

Q. Errera and R. Ménard

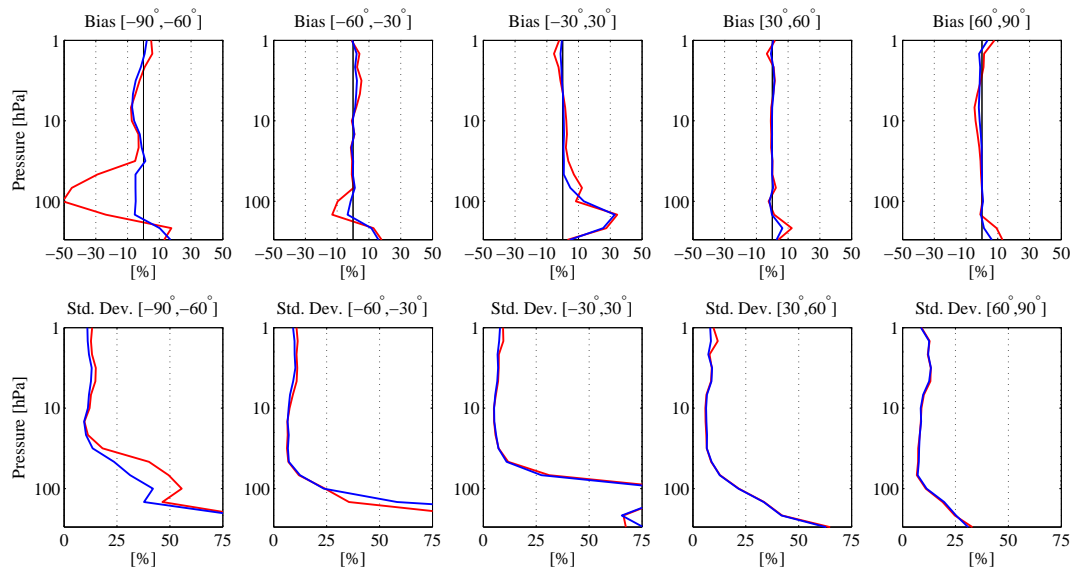


Fig. 3. Bias (top row) and standard deviation (bottom row) of the Observations-minus-Forecast (OmF) statistics between the analyses and the MIPAS data. Statistics are done at five latitude bands denoted in each title of each plot. Blue and red lines represent the statistics obtained, respectively, by the CORREL and DIAG runs.

[Title Page](#)
[Abstract](#)
[Introduction](#)
[Conclusions](#)
[References](#)
[Tables](#)
[Figures](#)
[⏪](#)
[⏩](#)
[◀](#)
[▶](#)
[Back](#)
[Close](#)
[Full Screen / Esc](#)
[Printer-friendly Version](#)
[Interactive Discussion](#)

**Spectral
representation of
background error
covariances**

Q. Errera and R. Ménard

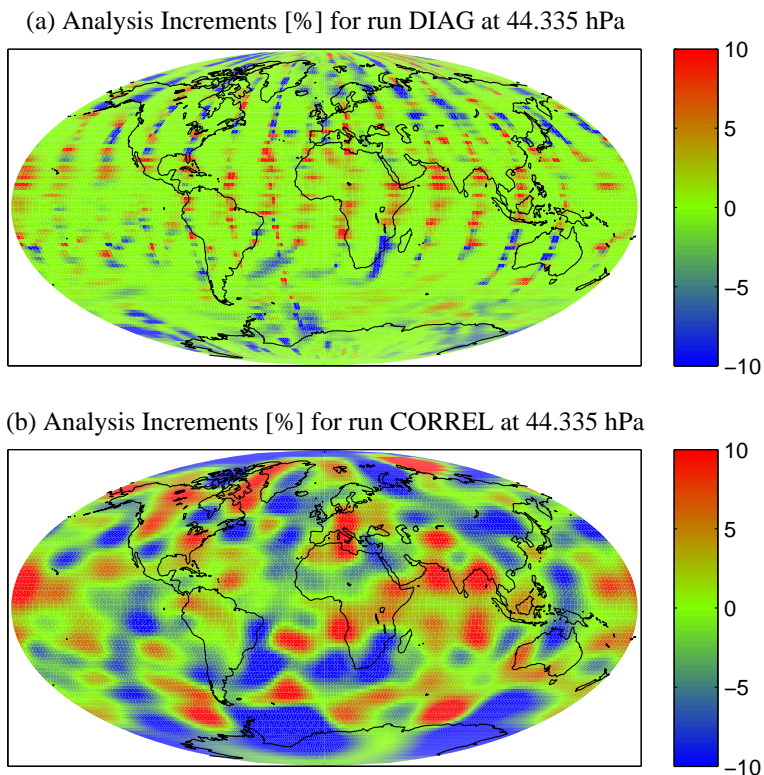


Fig. 4. Analysis increments of the runs DIAG (a) and CORREL (b) at the model level 21 (~ 44 hPa) on 15 September 2003. Blue and red indicate, respectively, negative and positive increments while green indicates close to zero increments.

Title Page

Abstract

Introduction

Conclusions

References

Tables

Figures

◀

▶

◀

▶

Back

Close

Full Screen / Esc

Printer-friendly Version

Interactive Discussion

**Spectral
representation of
background error
covariances**

Q. Errera and R. Ménard

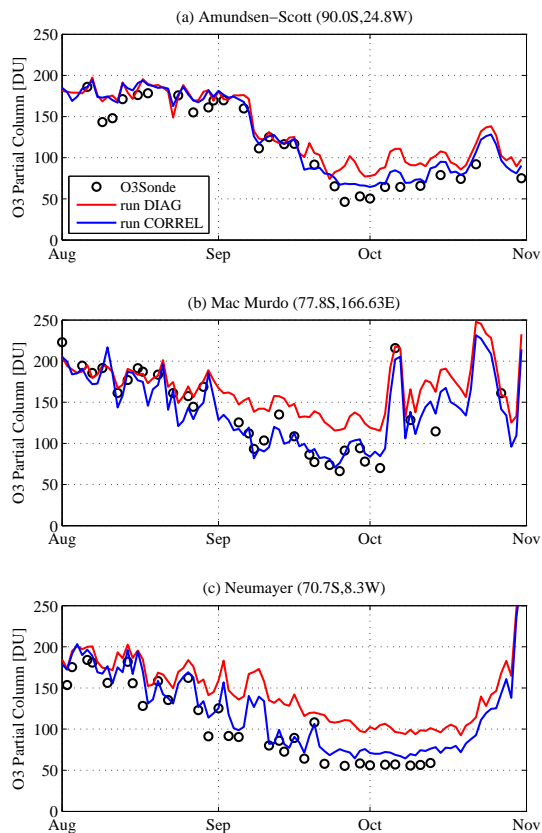


Fig. 5. Time series of the ozone partial column (10–100 hPa) between August and October 2003 obtained above three NDACC stations in Antarctica by the ozone sondes (black circles), and the runs DIAG (red line) and CORREL (blue line).

[Title Page](#)[Abstract](#)[Introduction](#)[Conclusions](#)[References](#)[Tables](#)[Figures](#)[◀](#)[▶](#)[◀](#)[▶](#)[Back](#)[Close](#)[Full Screen / Esc](#)[Printer-friendly Version](#)[Interactive Discussion](#)

**Spectral
representation of
background error
covariances**

Q. Errera and R. Ménard

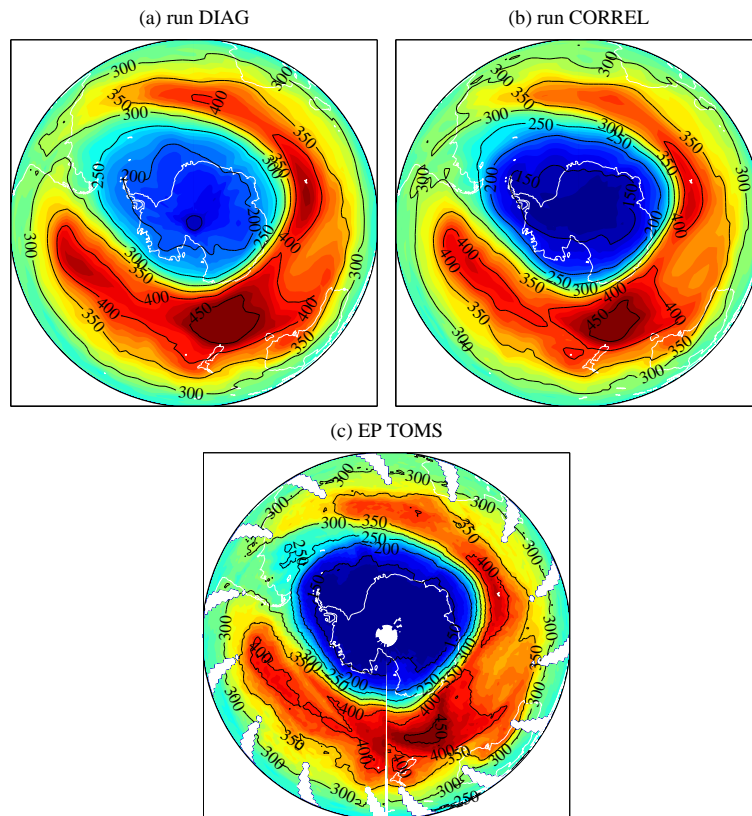


Fig. 6. Total ozone in the Southern Hemisphere on 1 October 2003 obtained by the runs DIAG (a) and CORREL (b), and observed by the Total Ozone Measurement Satellite (TOMS) (c).

Title Page

Abstract

Introduction

Conclusions

References

Tables

Figures

◀

▶

◀

▶

Back

Close

Full Screen / Esc

Printer-friendly Version

Interactive Discussion